Journal of Sustainable Metallurgy (2021) 7:858–873
https://doi.org/10.1007/s40831-021-00400-z

THEMATIC SECTION: 3RD INTERNATIONAL BAUXITE RESIDUE VALORISATION AND BEST PRACTICES CONFERENCE

Iron Recovery from Red Mud Using Carbothermic Roasting with Addition of Alkaline Salts

Pavel Grudinsky[1] · Dmitry Zinoveev[1,2] · Anfisa Yurtaeva[1,3] · Alex Kondratiev[2] · Valery Dyubanov[1] · Alexander Petelin[2]

Received: 17 March 2021 / Accepted: 1 July 2021 / Published online: 28 July 2021

Abstract

Red mud is a hazardous waste of alumina production by the Bayer method, which can be used for recovery of valuable elements such as iron, aluminum, titanium, and scandium. In this study, carbothermic roasting of red mud followed by dry or wet magnetic separation was applied with addition of alkaline salts to enhance iron extraction. A comparative influence of the use of sodium and potassium carbonates and sulfates, as well as the effects of roasting temperature and amounts of the additives on iron recovery and the iron concentrate grade were studied experimentally on two industrial red mud samples. The general mechanism of the roasting process in the presence of alkali metals was proposed in terms of temperature and iron extraction. Influence of the grinding fineness of the roasted samples and magnetic field strength during wet magnetic separation on iron extraction was also studied. It was shown that the addition of sodium and potassium carbonates and sulfates during carbothermic roasting of red mud improves the magnetic separation of metallic iron. The composition and microstructure of the separation products were examined, and their possible application was discussed.

Graphical Abstract

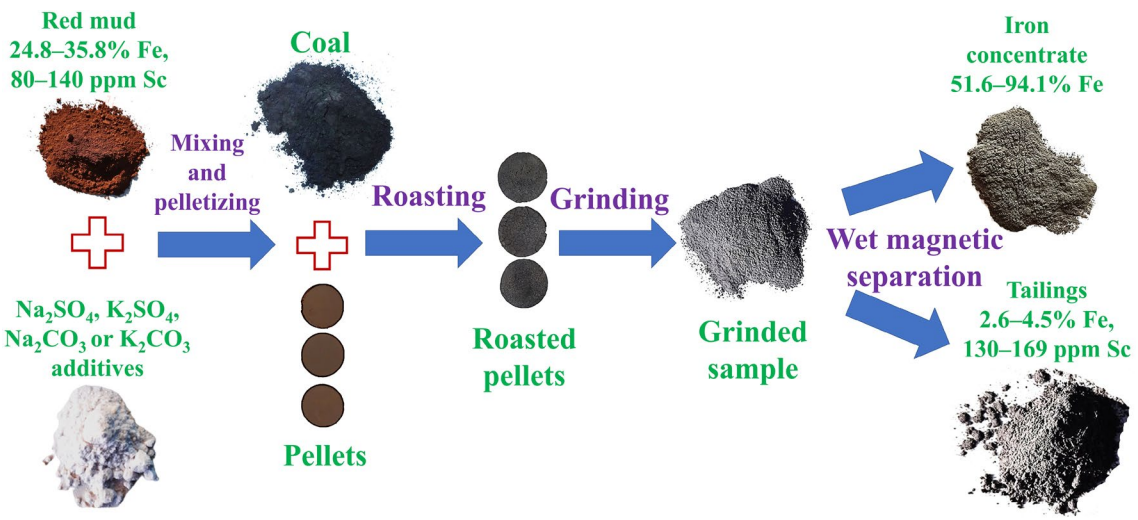

Keywords Red mud · Bauxite residue · Carbothermic roasting · Carbothermic reduction · Magnetic separation

The contributing editor for this article was Yiannis Pontikes.

✉ Pavel Grudinsky
pgrudinskiy@imet.ac.ru

Extended author information available on the last page of the article

Introduction

Currently, many different industrial wastes have been accumulating in the world [1, 2]. Metallurgy produces a wide range of products for various purposes and significantly contributes to the total amount of waste [3–6]. According to the sustainable practices in waste management [7], recycling is the preferred method in the case of impossibility to prevent or/and reuse waste produced in the process. The best world practices have demonstrated that metallurgical wastes can be recycled not only in related metallurgical plants, but also in other areas, for example, in construction [8–10] and chemical industry [11, 12], as well as in agriculture [13], etc. Recycling contributes not only to converting waste into valuable resources and to preventing economic and ecological expenses of landfilling, but also considerably facilitates saving of natural raw materials [14]. However, metallurgical industry still generates wastes that are recycled insignificantly: the "bauxite residue" or "red mud" is the example of such waste. Red mud is produced world-wide during bauxite processing by the Bayer method [15]; it contains 10–20% Al_2O_3, 3–50% SiO_2, 30–60% Fe_2O_3, 2–8% CaO, 0–25% TiO_2, and also up to 1% of total rare earth elements (REEs) expressed as oxides [16–18].

Many researchers have attempted to find out a cost-effective way of red mud recycling in different industries [19–21], but it led to a limited practical application [22]. There are studies to use red mud as catalyst [23, 24], coagulant and flocculant [25, 26], and adsorbent [27, 28]. Although these methods can be applied on an industrial scale, the red mud recycling would still be required due to its significant amount accumulated world-wide in comparison with the amount utilized by these methods. A number of studies have been carried out to utilize red mud in the construction industry with a high consumption of raw materials, namely, in production of cement [29], concrete [30], bricks [31], tiles [32], as well as in road construction [33]. From this perspective, the disadvantage of such methods is a loss of red mud components, which are valuable for metallurgy: e.g., REEs, due to their rapid demand increasing [34, 35], as well as iron, aluminum, titanium, etc. So far, the alumina industry has accumulated over 4.6 billion tons of red mud over the world [36], but only about 15% is recycled [37]; the rest is stored into sludge dumps. Russia, which is one of the main world alumina producers, has already accumulated nearly 600 million tons of red mud [38] and its amount increases by 5–8 million tons each year. Nonetheless, only a small amount of the Russian red mud storage is used to recover scandium [39] and to produce a pigment [40].

Iron is the main component of red mud [17]. Many methods have been proposed up to date for extraction of iron from this waste. For example, reduction smelting [41, 42], leaching by different acids [43, 44], carbothermic roasting with subsequent magnetic separation [45, 46], and high-intensity magnetic separation [47, 48] are widely investigated methods for iron extraction. Undoubtedly, the solid-phase carbothermic reduction is a more cost-effective method for iron extraction compared with the reduction smelting due to a lower process temperature. However, iron grains obtained by carbothermic reduction of red mud at 1000–1300 °C have a very small size and are attached to calcium aluminosilicate phases [49], which makes it difficult to separate iron from the gangue phase by magnetic separation. Special additives to the red mud are required in this approach to enhance iron extraction. These additives promote reduced iron growth that facilitates gangue-grain release [50] during fine grinding and thereby consequently improve the magnetic separation. Traditionally, the sodium salts are used, namely, carbonate and sulfate [51–53]. Our previous works [54–56] have shown that the addition of sodium and potassium salts for carbothermic reduction of red mud promotes growth of iron grains and improves the magnetic separation efficiency.

The present paper continues our investigation of the effects of addition of alkali carbonates and sulfates on iron recovery. This paper presents the results of K_2SO_4 addition and summarizes the influence of Na_2SO_4, Na_2CO_3, and K_2CO_3, as well as roasting temperature, on the carbothermic solid-phase reduction of red mud samples obtained from two different Russian (Bogoslovsky and Ural) aluminum plants with basicity (CaO/SiO_2) of 0.46 and 1.21, respectively. The iron grain growth and dry magnetic separation efficiency as well as the effects of other parameters such as the roasting temperature, grinding fineness, and magnetic field strength during wet magnetic separation were studied experimentally. The iron concentrates and tailings obtained during carbothermic reduction were also analyzed and compared to each other.

Materials and Methods

Red Mud Samples Characterization

The red mud samples from Bogoslovsky Aluminum Plant (Krasnoturyinsk, Russia) and Ural Aluminum Plant (Kamensk-Uralsky, Russia) were used in the experiments. Sodium was removed from the Ural Aluminum plant sample by leaching with a lime slurry in a glass reactor at 90 °C for 3 h [57]. The chemical composition of red mud was analyzed by an X-ray fluorescence spectrometer PANalytical AXIOSmax Advanced (Netherlands). The X-ray diffraction (XRD) patterns were obtained by an X-ray diffractometer ARL X'TRA (Switzerland) with Cu-K_α radiation source. Table 1 shows the chemical composition of the samples. The

Table 1 Chemical composition of red mud taken from different plants (wt%)

Red mud sample	Fe	Si	Al	Ti	Ca	Mg	Mn	Na	P	S	Sc
Ural	25.8	4.07	6.25	2.12	17.1	0.61	0.74	0.2	0.18	0.14	0.008
Bogoslovsky	34.8	4.07	6.76	2.8	6.62	0.4	0.2	2.45	0.38	0.48	0.014

Table 2 Composition of the systems for thermodynamic simulation (g)

Red mud sample	SiO_2	Al_2O_3	CaO	Na_2O/K_2O
Ural	21	26	53	0–20
Bogoslovsky	28	42	30	

XRD patterns of the red mud samples are published in our previous paper [56].

It can be seen that the Ural red mud sample contains more calcium and less other elements than the Bogoslovsky red mud due to the preliminary treatment. Consequently, the Ural red mud has a rather different mineralogy owing to an increased amount of calcium-containing minerals such as calcite and portlandite.

Thermodynamic Simulation

Thermodynamic simulation of phase equilibrium of the red mud-alkaline salts system was carried out by FactSage 8.0 software (Germany/Canada) using FToxide database [58]. The model system was based on a simplified red mud composition (only major oxides were taken into account; it was accepted that the all iron-containing phases were fully reduced to metallic iron) with addition of K_2O or Na_2O. The composition of each model system was determined as follows. The weight contents of Si, Ca, and Al, which have the same ratio as in the original red mud samples, were converted into the oxides and normalized to 100 g. Afterward, Na_2O or K_2O in the range of 0-20 g were added to 100 g of these normalized red mud samples. The resulted compositions that represent the $CaO–Al_2O_3–SiO_2–Na_2O$ and $CaO–Al_2O_3–SiO_2–K_2O$ systems are given in Table 2.

Experiments

The carbothermic roasting experiments were realized in a muffle furnace at the temperature range of 1000–1400 °C during 1–3 h. Long-flame coal was applied as a reductant; it contains about 15% of ash and 18% of moisture. The salt additives were chemically pure reagents of Na_2SO_4, K_2SO_4, Na_2CO_3, and K_2CO_3. The samples were quenched after roasting into liquid nitrogen to prevent secondary oxidation, ground and sieved to the required fineness, and then magnetic separation was performed. The roasted samples were ground using a microgrinder Fritsch Pulverisette 7 premium line (Germany), grinding machine DF-4 (China), or a jasper mortar with a pestle depending on the required fineness degree. Particle size classification was performed by a vibrating screen. Dry magnetic separation was carried out by drum BSMK-200 (Russia) device with the magnetic field density of 0.35 T. Wet magnetic separation was realized by XCGS-50 (China) device (Davis tube) with the magnetic field density in the range of 0.05–0.45 T. A sample for wet magnetic separation of 5–8 g in weight of required grinding fineness was placed into the device, which was filled by tap water, with preset required intensity of magnetic field and was separated using flowing tap water.

The microstructure of the roasted samples was analyzed by an optical microscope METAM LV-34 (Russia). Iron grain size was calculated from micrographs using the Image Pro Plus software (USA). The detailed methodology of the experimental procedure and calculation of iron grain size was described in our previous studies [55, 56]. Figure 1 demonstrates a schematic diagram of the roasting experimental procedure.

The total iron content was determined by an atomic absorption spectrometer Varian AA240FS (Australia) after

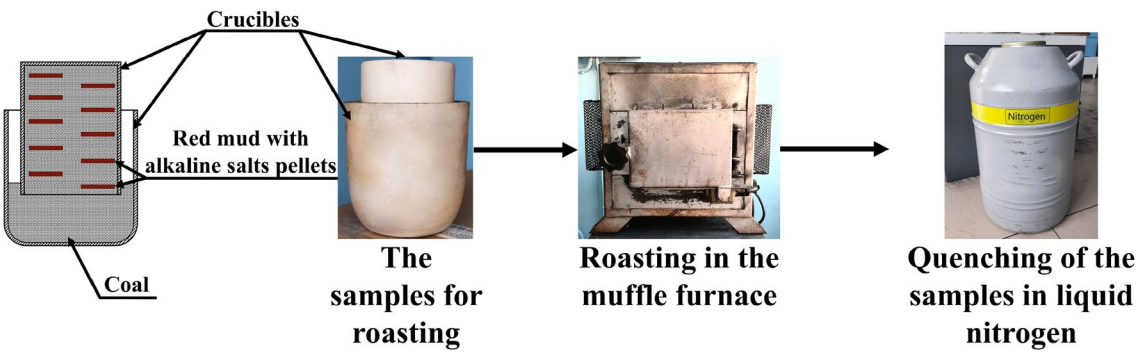

Fig. 1 Experimental procedure of the carbothermic roasting

alkaline fusion and acid digestion or only acid digestion of the samples. The alkaline fusion was used for the majority of the roasted samples. When the iron content was more than 30%, complexometric titration method for total iron analysis was applied using 0.025 M Trilon solution and 20–25% sulfosalicylic acid as an indicator at pH 2–3 until the color change from blue violet to lemon yellow is seen. The metallic iron content in the samples was analyzed by the potassium dichromate titration method after selective leaching of metallic iron using a $FeCl_3$ solution [59].

Results and Discussion

Thermodynamic Calculation

Figures 2 and 3 show the polythermal sections of the equilibrium phase diagrams of the $CaO–Al_2O_3–SiO_2–Na_2O$ and $CaO–Al_2O_3–SiO_2–K_2O$ systems, respectively, which are resulted from addition of alkaline salts to the Ural and Bogoslovsky red mud samples. Figure 2 indicates that the addition of Na_2O first decreases the system solidus (i.e., the curve, at which a liquid first appears, shown on the figure as a red line). For the Ural red mud, (Fig. 2a) the liquid phase first appears in the system at temperature of above 1450 °C without Na_2O addition, while addition of 1–6% of Na_2O lowers the solidus temperature down to 1300 °C. A further increase of Na_2O to 6–8% leads to a sharp increase of the system solidus, while Na_2O addition of more than 8% decreases the solidus to 1150 °C. For the Bogoslovsky red mud (Fig. 2b) the liquid phase first appears at 1400°C and addition of approximately 2–10% of Na_2O lowers the solidus down to 1240–1260 °C. A further addition of Na_2O decreases the system solidus to about 1100 °C.

Figure 3a, b illustrates the effect of the K_2O addition on the Ural and Bogoslovsky red mud system solidus. For the Ural red mud (Fig. 3a), addition of K_2O of more than 1% generally lowers the solidus from about 1450 to 1300 °C. However, for the Bogoslovsky red mud the solidus with K_2O addition (Fig. 3b) decreases first from 1400 to 1300 °C (K_2O < 8%), then increases to above 1400 °C (8–13% K_2O), and then decreases again to 1300 °C (K_2O > 13%).

Iron Grain Size

Our previous works [55, 56] have shown that iron-containing phases present in red mud can almost completely be reduced to metallic iron at 1100–1200 °C. However, it is impossible to separate iron from the gangue phase using mechanical grinding followed by magnetic separation due to small sizes of iron grains and their dissemination with gangue. Microstructure investigation of the roasted samples from Ural aluminum plant without additions showed that iron grains were mainly of 1–20 μm in size. The addition of Na_2CO_3 or K_2CO_3 leads to a considerable iron grain growth without increasing temperature. To obtain similar in size iron grains without salt addition, the process temperature should be increased to 1400 °C.

Figure 4 compares the iron grain size after the carbothermic roasting of red mud with 13.7% Na_2SO_4 and 19% K_2SO_4 in the samples obtained from Ural and Bogoslovsky plants, respectively. The bar charts show that an increase of temperature leads to iron grain growth for both the Ural and Bogoslovsky red mud samples. However, the relative area of iron grains larger than 40 μm is more than 70% already at 1200 °C in the Bogoslovsky red mud sample, while the same results in the Ural red mud sample can be obtained only at 1400 °C likely due to different basicity of the red mud samples.

The addition of 19% K_2SO_4 increases iron grain size in both the samples, as well as sodium sulfate, but at different temperature ranges. The relative area of iron grains larger than 40 μm is only 50% at 1400 °C for the Ural sample, while the percentage of the largest fraction reaches 55% already at 1250 °C. It sharply increases to 95% at 1300 °C for the Bogoslovsky sample.

In this way, the Bogoslovsky sample is more favorable for the carbothermic roasting because the additions of sodium and potassium sulfates increase the relative area of iron grains larger than 40 μm at significantly lower temperatures than those for the Ural sample.

Figure 5 demonstrates the effect of roasting temperature at the range of 1200–1400 °C on the relative area of iron grains with a size larger than 40 μm without addition, as well as with the additions of 17.1% Na_2CO_3 and 17.6% K_2CO_3, respectively. The graph shows that both the additions enlarge the iron grains. The addition of 17.1% Na_2CO_3 leads to increasing the grain size more effectively than 17.6% K_2CO_3; this difference is due to a lower melting temperature of the gangue phase with Na_2CO_3 addition than that with the addition of K_2CO_3, which is consistent with the calculated phase diagrams (Figs. 2, 3). The iron grain size correlates well with the amount of liquid phase. It can be seen from the graphs that the liquid phase as well as large iron grains are still absent in the sample without additions at 1200–1250 °C. The relative area of iron grains larger than 40 μm with the addition of sodium carbonate at 1300 °C and 1350 °C is already over 50% and about 97%, respectively, due to the amount of the liquid phase increasing with rising of temperature. The relative area of iron grains larger than 40 μm also sharply increases with a further increase in the liquid phase amount. It should be noted that although an increase of the liquid phase amount promotes iron grain growth and improves iron extraction from red mud, it can impose limitations for practical realization of the approach in some metallurgical units developed for solid-phase processes,

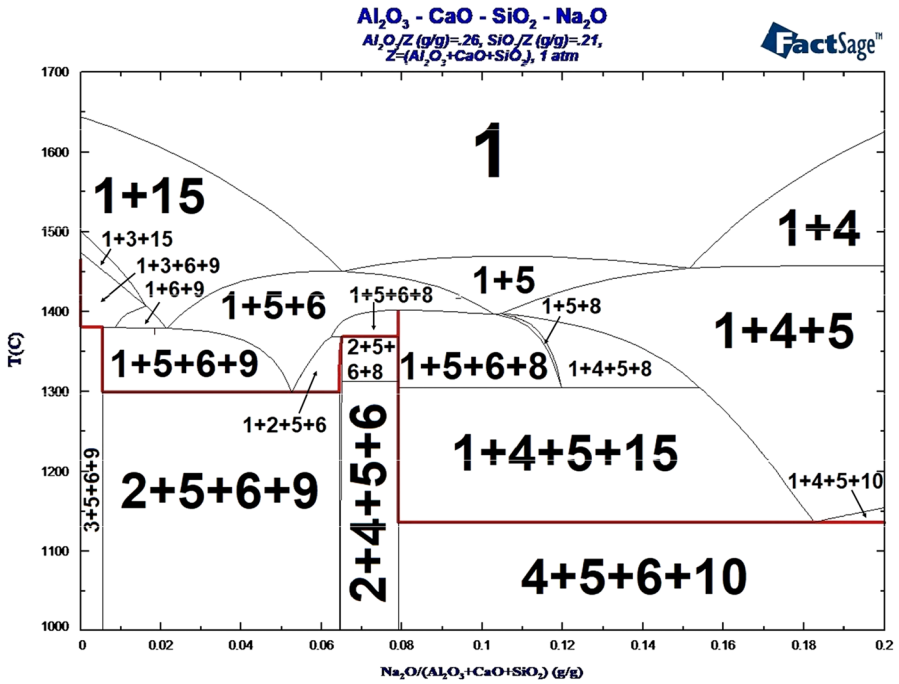

(a)

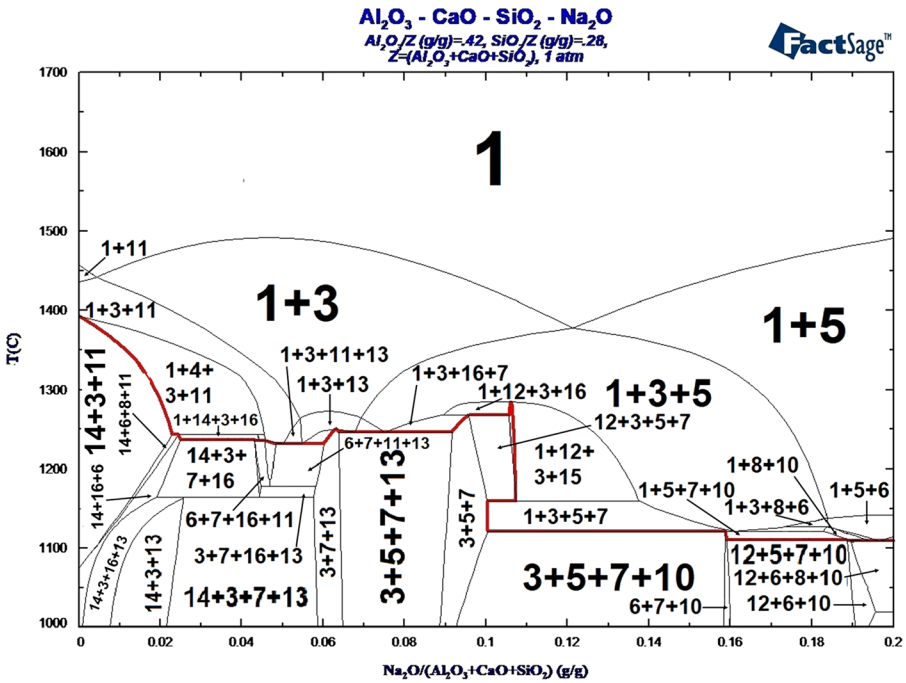

(b)

Fig. 2 The phase equilibrium diagrams $CaO–Al_2O_3–SiO_2–Na_2O$ for Ural (**a**) and Bogoslovsky (**b**) sample, where 1, liquid phase; 2, $Ca_3Al_2O_6$; 3, $(Ca,Na)_2Al(Si,Al)_2O_7$ (melilite); 4, CaO; 5, $Na_2CaAl_4O_8$; 6, Ca_2SiO_4(α-prime); 7, $NaAlSiO_4$; 8, Ca_3SiO_5; 9, $CaAl_2O_4$; 10, Na_2CaSiO_4; 11, $CaAl_{12}O_{19}$; 12, $NaAlO_2$; 13, $Na_2Ca_3Al_{16}O_{28}$; 14, $NaAlSi_3O_8$; 15, Ca_2SiO_4(α); and 16, Al_2O_3. Solidus line is highlighted as red (Color figure online)

in particular, due to formation of incrustation in tube-type furnaces, so the amount of liquid phase should stay within certain limit determined experimentally

Figure 6 shows the photomicrographs of the Ural red mud sample after the roasting at various temperatures without additives and with the addition of 17.6% K_2CO_3, respectively. The microphotographs correlate very well with Fig. 5. The images clearly show that the addition of 17.6% K_2CO_3 improves the growth of iron grains. Despite the fact that most of iron grains are small at 1100–1200 °C in both samples without and with additions, the distribution of iron particles is different. A distance between iron particles in

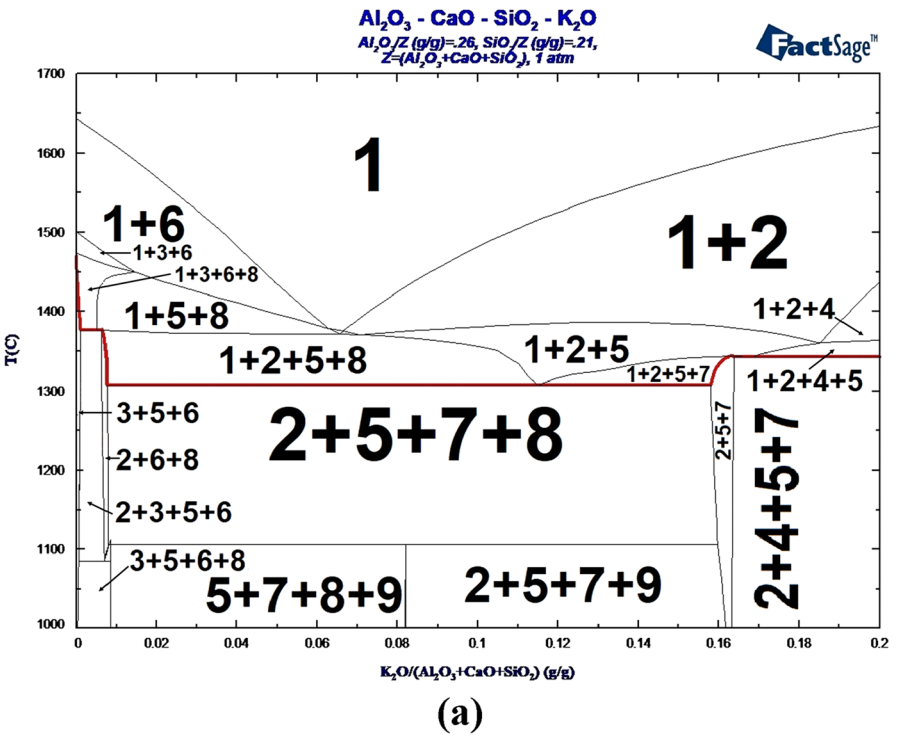

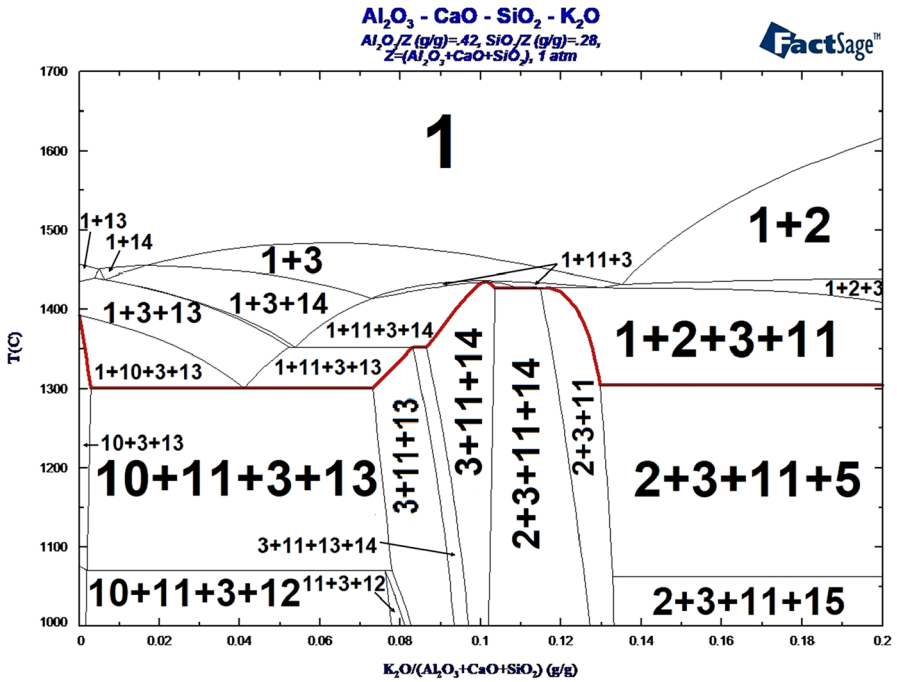

Fig. 3 The phase equilibrium diagrams $CaO–Al_2O_3–SiO_2–K_2O$ for Ural (**a**) and Bogoslovsky (**b**) sample, where 1, liquid phase; 2, $KAlO_2$; 3, $(Ca,Na)_2Al(Si,Al)_2O_7$ (melilite); 4, CaO; 5, Ca_2SiO_4(α-prime); 6, Ca_2SiO_4(α); 7, $Ca_3Al_2O_6$; 8, $CaAl_2O_4$; 9, $K_4Ca_3Al_{10}O_{20}$; 10, feldspar $KAlSi_3O_8–CaAl_2Si_2O_8$; 11, $KAlSiO_4$; 12, Al_2O_3; 13, $CaAl_{12}O_{19}$; 14, $CaAl_4O_7$; and 15, $K_2Ca_6Si_4O_{15}$. Solidus line is highlighted as red (Color figure online)

the samples with K_2CO_3 addition is larger compared to the sample without addition. Moreover, several areas with a high concentration of iron particles were discovered in the sample with additive. At 1300 °C, the relative area of iron grains larger than 40 µm is 35% with the addition of 17.6% K_2CO_3, while without addition it is 14%.

Figure 7 demonstrates photomicrographs of the Bogoslovsky red mud sample after the roasting at 1100–1200 °C with the addition of 18.2% Na_2SO_4. The grain shapes are different compared with Fig. 6 that is likely due to a different mechanism of iron grain growth between the roasting with the sulfates and the carbonates. As can be seen, rather large iron particles are generated during the roasting of the Bogoslovsky red mud with sodium sulfate at lower temperatures; therefore, we used the Bogoslovsky sample roasted with the addition of 18.2% Na_2SO_4 at 1150 °C for the following investigation of magnetic separation process.

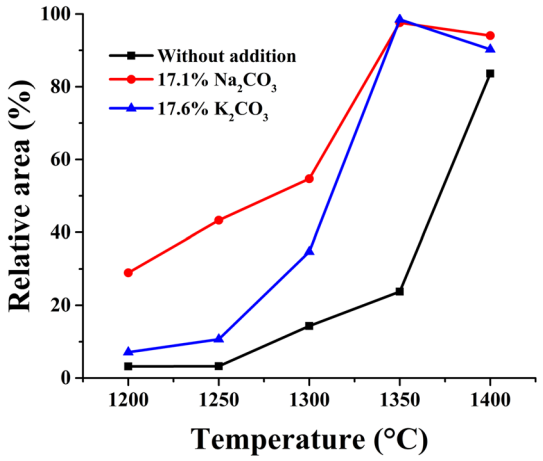

Fig. 5 Effect of temperature on the relative area of iron grains larger than 40 µm after 3-h carbothermic roasting of red mud without addition, with 17.1% Na_2CO_3 and 17.6% K_2CO_3 from Ural aluminum plant

Magnetic Separation

It has shown in our previous work [56] that the iron concentrate with 58.3% Fe can be obtained after carbothermic roasting of the Bogoslovsky red mud with 18.2% Na_2SO_4 at 1150 °C and dry magnetic separation. The additional study using wet magnetic separation process was performed to improve the iron concentrate grade.

Figure 8 shows an influence of the grinding fineness (Fig. 8a) and magnetic field density (Fig. 8b) during wet magnetic separation on the iron concentrate grade and iron recovery, respectively. Figure 8a illustrates that the iron grade slowly rises with an increase of the yield of particles − 0.033 mm. The iron recovery degree is more than 80% across the entire range of grinding fineness. As can be seen,

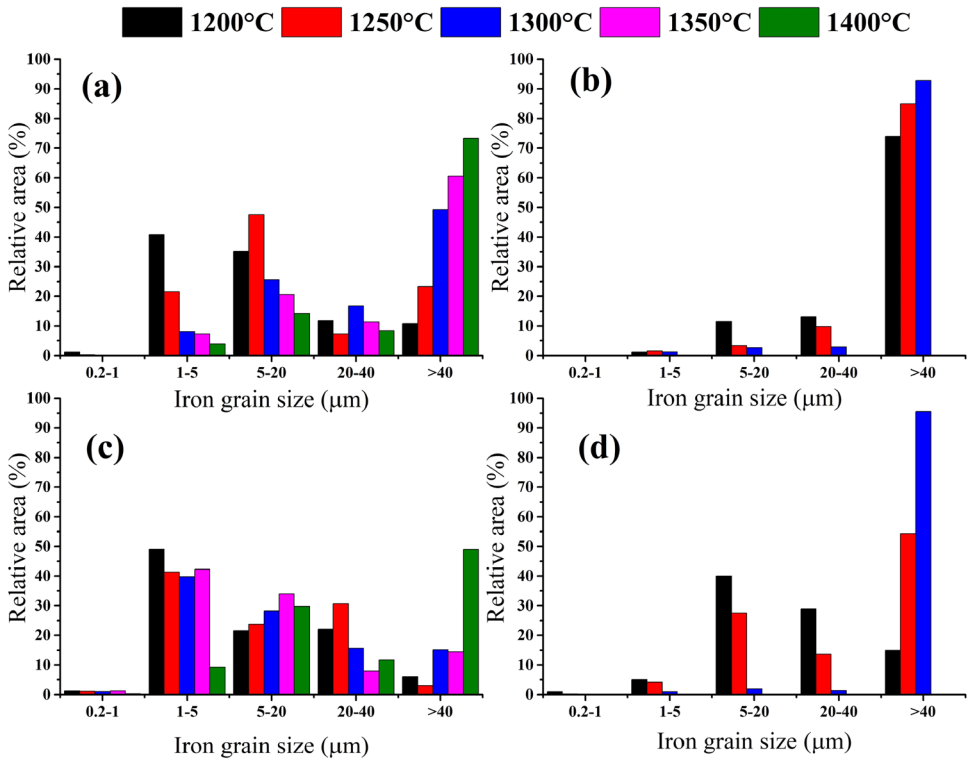

Fig. 4 Effect of temperature on the relative area of iron grains of different fractions after 3-hour carbothermic roasting of the Ural (**a**) and Bogoslovsky (**b**) red mud with 13.7% Na_2SO_4 and of the Ural (**c**) and Bogoslovsky (**d**) red mud with 19% K_2SO_4, respectively

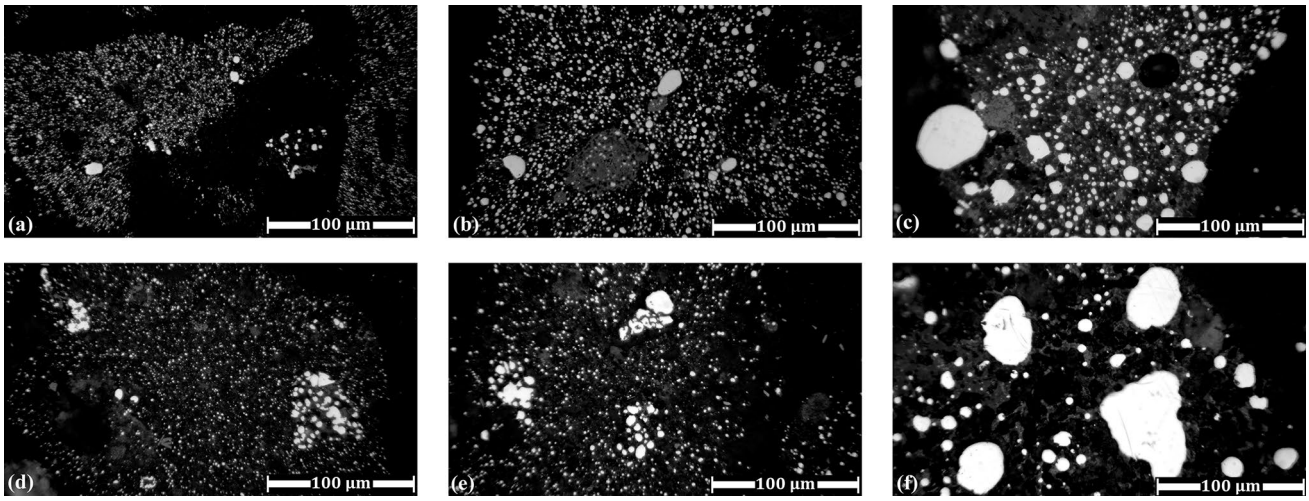

Fig. 6 Photomicrographs of the roasted red mud samples from Ural aluminum plant for 3 h at 1100 °C (**a**), 1200 °C (**b**), and 1300 °C (**c**) without additions, as well as at 1100 °C (**d**), 1200 °C (**e**), and 1300 °C (**f**) with 17.6% K_2CO_3

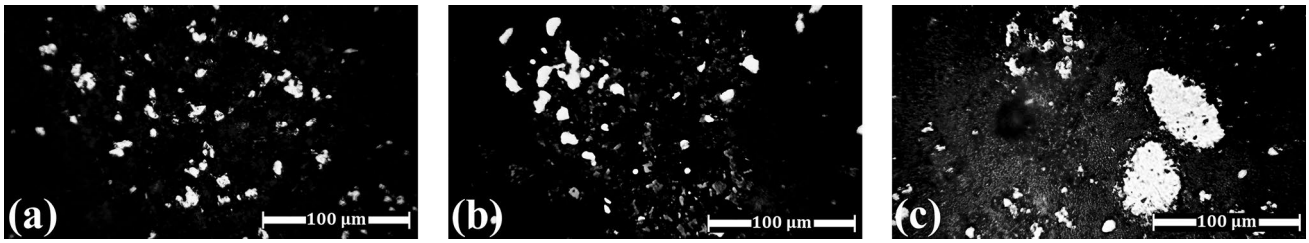

Fig. 7 Photomicrographs of the roasted red mud samples from Bogoslovsky aluminum plant with 18.2% Na_2SO_4 for 3 h at 1100 °C (**a**), 1150°C (**b**), and 1200°C (**c**)

the iron grade is 73%, and the iron recovery is 92% at a maximum grinding fineness. Figure 8b demonstrates that the iron grade is almost constant in the range of 0.05–0.25 T and decreases at 0.35 T that makes it unnecessary to increase the magnetic induction above 0.25 T. The iron recovery degree at the covered range of magnetic field varies from 80 to 90%. Thus, the optimal conditions for the wet magnetic separation are the degree of grinding − 0.033 mm of 94.8% and the value of magnetic induction of 0.15 T, where the iron grade is 76.7%, and iron recovery degree is 90.09%. Therefore, the wet separation has a higher efficiency than the dry magnetic separation for the roasted sample at 1150 °C. However, dry magnetic separation also led to producing quite high-grade concentrates for the samples obtained at 1200–1350 °C. Table 3 indicates a dry magnetic separation efficiency of such roasted samples. The results also show that iron extraction is considerably easier from the Bogoslovsky red mud sample than from the Ural one. The roasting of the Bogoslovsky red mud with 9.1% Na_2SO_4 at 1250 °C led to obtaining of iron concentrate with both the iron recovery and iron grade percentages above 90%, while these indexes for the roasted Ural red mud at 1350 °C with 15% Na_2SO_4 were 87.2% and 51.6%, respectively.

Figure 9 shows the effect of the roasting temperature on the iron recovery and iron grade of the obtained concentrates. At lower temperatures with the addition of 17.1% Na_2CO_3 and 22% K_2CO_3, there were no separation into a concentrate and tailings. Na_2CO_3 and K_2CO_3 addition to the

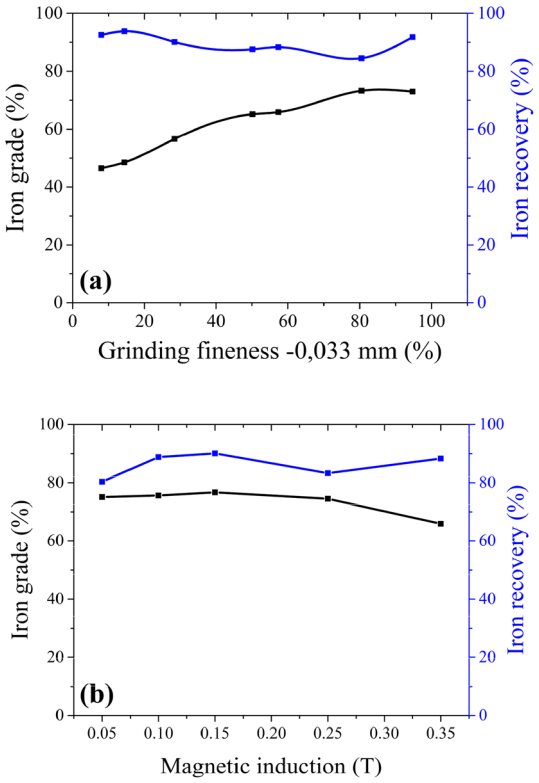

Fig. 8 Effect of grinding fineness − 0.033 mm at 0.35 T **(a)** and magnetic field at degree of grinding − 0.033 mm of 57.4% (= − 0.05 mm of 100%) (**b**) on the iron grade and iron recovery during wet magnetic separation of the Bogoslovsky red mud with 18.2% Na_2SO_4 addition roasted at 1150 °C for 1 h

Ural red mud resulted in a rather high recovery degree, as well as in 95% and 94% of the iron grade, respectively. Figure 9 shows a temperature influence on the indexes of dry magnetic separation after carbothermic roasting of Ural red mud at the optimal amounts of Na_2CO_3 and K_2CO_3 addition according to our previous paper [55]. It can be seen that the additions of Na_2CO_3 and K_2CO_3 lead to a high iron separation already at 1250–1300 °C. Furthermore, it is interesting to note that the addition of K_2CO_3 improves the efficiency of dry magnetic separation at a lower temperature compared with Na_2CO_3. Nevertheless, the efficiency of dry magnetic separation of the samples with Na_2CO_3 addition at 1350–1400 °C is higher than with K_2CO_3 addition.

The iron grade and iron recovery degree depend strongly on temperature, as also demonstrated in our previous work [56]. Based on the results of multifactorial analysis of the carbothermic roasting—magnetic separation process, Table 4 explains the mechanism of the temperature effect on the indexes of dry magnetic separation in the case of Fig. 9.

Table 5 shows the general mineralogical composition of the Ural red mud after 3-h roasting at 1000–1200 °C without and with the addition of different alkaline salts. It should be noted that the quantitative phase composition is almost similar for a certain additive at the temperature and the addition amount ranges. All the samples contain mainly aluminum and calcium minerals such as gehlenite, mayenite, perovskite, dicalcium, and tricalcium silicates; the iron-containing phases are metallic iron and Fe–C alloy. The particular phases of the samples with the sulfate additions are CaS and FeS, which have both a favorable and unfavorable influence on the roasting and magnetic separation processes depending on the sample basicity [56]. Although they significantly reduce the temperature of liquid phase appearance, facilitate grinding due to iron grain growth acceleration by FeS formation, calcium sulfide increases the melting point of the sample, thereby hindering the grain growth process. However, although FeS has a favorable effect on iron grain growth during the roasting, iron recovery and iron content

Table 3 Efficiency of dry magnetic separation for the roasted red mud samples during 3 h

Roasting conditions	Addition	Red mud sample	Iron recovery (%)	Iron grade (%)	Metallization degree (%)	Iron in tailings (%)
1350°C, 3 h	22% K_2CO_3	Ural	81.05	95	98.24	1.97
	17.1% Na_2CO_3	Ural	86.69	94.1	99.51	4.29
	27.3% Na_2SO_4	Ural	87.2	51.6	96.92	4.64
1250°C, 3 h	9.1% Na_2SO_4	Bogoslovsky	90.06	90.8	98.41	2.96
1300°C, 3 h	14.2% K_2SO_4	Ural	87.62	60.72	98.80	7.02
	19% K_2SO_4	Bogoslovsky	85.68	92.4	97.08	2.72
1200°C, 3 h	27.3% Na_2SO_4	Bogoslovsky	83.97	85.1	89.69	3.93

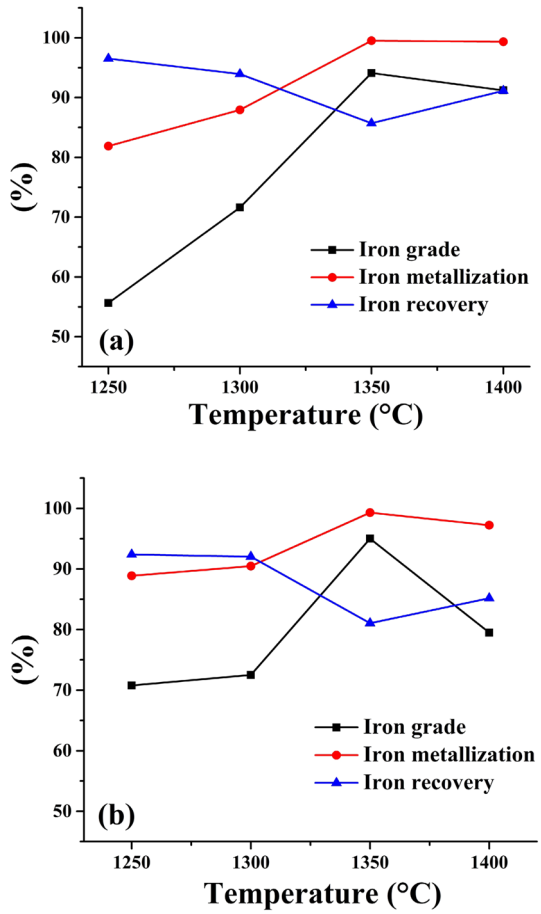

Fig. 9 Effect of temperature on the indexes of dry magnetic separation of Ural red mud sample with 17.1% Na_2CO_3 addition (**a**) and 22% K_2CO_3 addition (**b**)

in the concentrate decrease owing to partial remaining of iron sulfide in the tailings. Sodium carbonate addition led to $NaAlSiO_4$ and $MgAl_2O_4$ formation during the roasting, while potassium carbonate caused the formation of mainly water-soluble $KAlO_2$ with minor quantity of $KAlSi_2O_6$; it makes for more simple aluminum recovery from the tailings with the application of potassium salts by water leaching.

Figure 10 illustrates the XRD diffraction patterns of the samples without and with addition of Na_2CO_3 and K_2CO_3, respectively, which confirm the described mineralogical composition.

The application of Na_2CO_3 and Na_2SO_4 for the roasting of the highly basic Ural red mud led to the formation of such aluminum minerals as gehlenite, nepheline, and mayenite in the absence of sodium monoaluminate, while the addition of K_2CO_3 and K_2SO_4 resulted in a partial transformation of aluminum into potassium monoaluminate that is highly soluble in water [60]. Thermodynamic calculations also demonstrated that sodium monoaluminate is not formed in the Ural red mud (see Fig. 2a), while the presence of potassium monoaluminate (phase 2) can be seen in Fig. 3a. It indicates that the application of the potassium salts is more promising for subsequent aluminum extraction.

Figures 11 and 12 demonstrate the SEM images with the distribution of elements in the concentrate and the tailings obtained after the roasting of the Bogoslovsky red mud with 18.2% Na_2SO_4 at 1150 °C for 1 h and subsequent wet magnetic separation. Table 6 gives the results of the local SEM-EDX analysis of the concentrate and the tailings samples. The concentrate consists of iron metallic particles impregnated with gangue. SEM-EDX analysis of point no. 1

Table 4 General mechanism of the effect of the roasting temperature on the indexes of dry magnetic separation

Temperature (°C)	Iron grade (%)	Iron recovery (%)	Description
< 1250	n/s	n/s	Iron grains are small, separation from the gangue is impossible
1250–1300	55–73	92–96	Growth of iron grains is insignificant; a small proportion of the gangue-grain release occurs
1300–1350	Sharply increases up to 94–95	Decreases to 80–85	The liquid phase proportion increases, thereby contributing to aggregation of iron grains, as a result the iron grade rises sharply. Iron recovery decreases because small iron grains remain associated with the gangue after grinding of a partially molten material
1350–1400	Decreases to 80–90	Increases to 85–91	Iron recovery rises due to a decrease of the proportion of small grains as the liquid phase grows, captures the gangue particles, thereby leading to a decrease of the iron grade
> 1400	–	–	Strong melting effects. Segregation of iron grains into a single ingot

Table 5 Mineralogical composition of roasted Ural red mud samples at 1000–1200 °C for 3 h without and with addition of alkaline salts

Phases	No addition	Na_2SO_4 addition	K_2SO_4 addition	Na_2CO_3 addition	K_2CO_3 addition
General	$Al_2Ca_2SiO_7$, $12CaO{\bullet}7Al_2O_3$, $CaTiO_3$, Fe_xC_y, Fe, Ca_3SiO_5, Ca_2SiO_4				
Particular	–	CaS, FeS, $NaAlSiO_4$	CaS, FeS, $KAlO_2$, $KAlSi_2O_6$	$NaAlSiO_4$, $MgAl_2O_4$	$KAlO_2$, $KAlSi_2O_6$

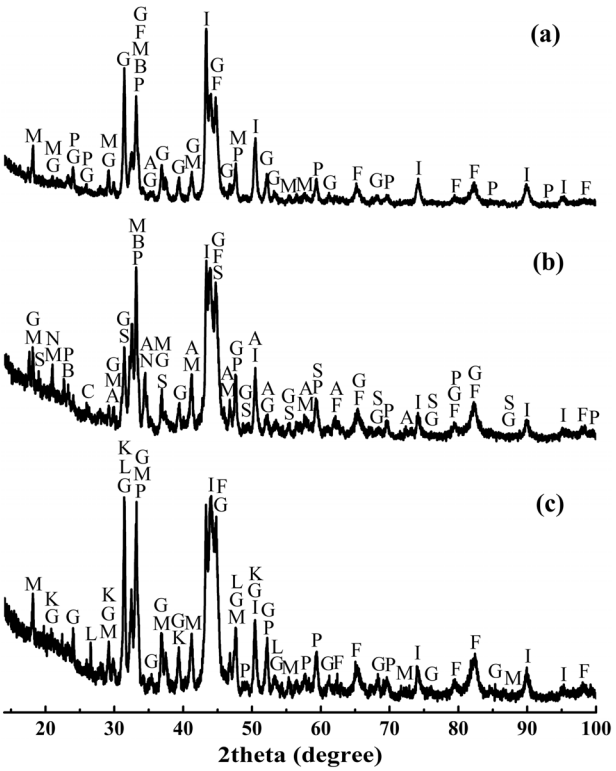

Fig. 10 The XRD patterns of roasted Ural red mud at 1100 °C for 3 h without additions (**a**), with 12.8% Na_2CO_3 (**b**), and with 13.2% K_2CO_3 (**c**), where G, $Al_2Ca_2SiO_7$; M, $12CaO•7Al_2O_3$; P, $CaTiO_3$ (perovskite); A, Ca_3SiO_5; I, Fe; F, $Fe_{1.92}C_{0.88}$; B, Ca_2SiO_4; S, $MgAl_2O_4$; N, $NaAlSiO_4$; L, $KAlSi_2O_6$; and K, $KAlO_2$

indicates the presence in the concentrate of the gangue particle, which contains CaS. The analysis of point no. 2 shows that iron is associated with phosphorus and sulfur, which is unfavorable due to following hinderance of the application of the concentrate in steel or ironmaking [61]. SEM analysis of the tailings (Fig. 12) indicates the association of iron and sulfur in sulfide form that predetermines iron losses with tailings during the magnetic separation process. Zirconium-scandium particle was found (Fig. 12, point no. 3), which is consistent with the other paper [62].

Table 7 indicates the chemical composition of the magnetic concentrates obtained at different conditions for the Bogoslovsky red mud without and with Na_2SO_4 addition.

Analysis of the chemical composition shows that iron content in the tailings is rather low, so the subsequent recovery of aluminum, titanium, and scandium by hydrometallurgical methods becomes more favorable compared with the initial red mud samples. The concentrate obtained using sodium sulfate as an additive contains a considerable sulfur percentage. The main part of phosphorus passed into the concentrate for both the samples. Furthermore, it is interesting to note that carbon content in the sample with Na_2SO_4 addition is higher than in the sample without additions.

Table 6 General composition (at.%) at the sampling points marked in Figs. 11 and 12

No.	O	Ca	Al	Si	Na	Ti	Fe	S	K	P	Zr	Sc	Mg	V
1	70.5	11.8	6.4	4.8	3	2.1	0.9	0.3	0.2	–	–	–	–	–
2	11.7	–	–	–		–	73.1	–	–	15.3	–	–	–	–
3	68.1	4.4	2.8	1.2	2.1	5	2.3	4.3	–	–	7.9	1.3	0.4	0.2

Table 7 Chemical composition of iron concentrate and tailings obtained under different conditions

Roasting conditions		Fe	C	P	S
1300 °C, without addition	Concentrate	87.6	0.75	0.85	0.018
	Tailings	2.6	n/d	0.074	0.44
1150 °C, 18.2% Na_2SO_4	Concentrate	74.2	1.65	0.98	1.29
	Tailings	4.50	n/d	0.057	4.77

n/d no data

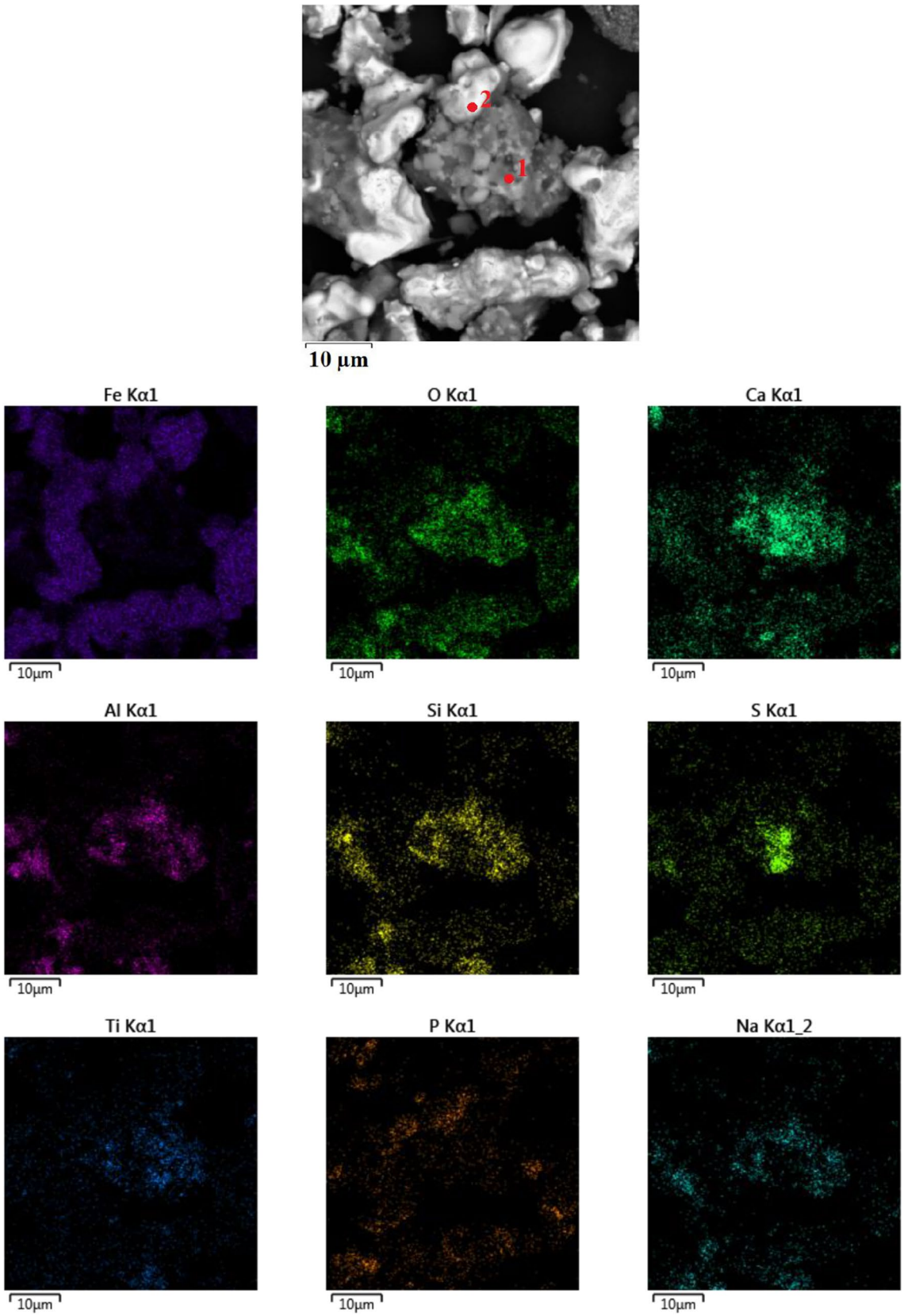

Fig. 11 SEM image with the distribution of elements in the concentrate obtained after the roasting of the Bogoslovsky red mud with 18.2% Na_2SO_4 at 1150 °C for 1 h followed by wet magnetic separation (Color figure online)

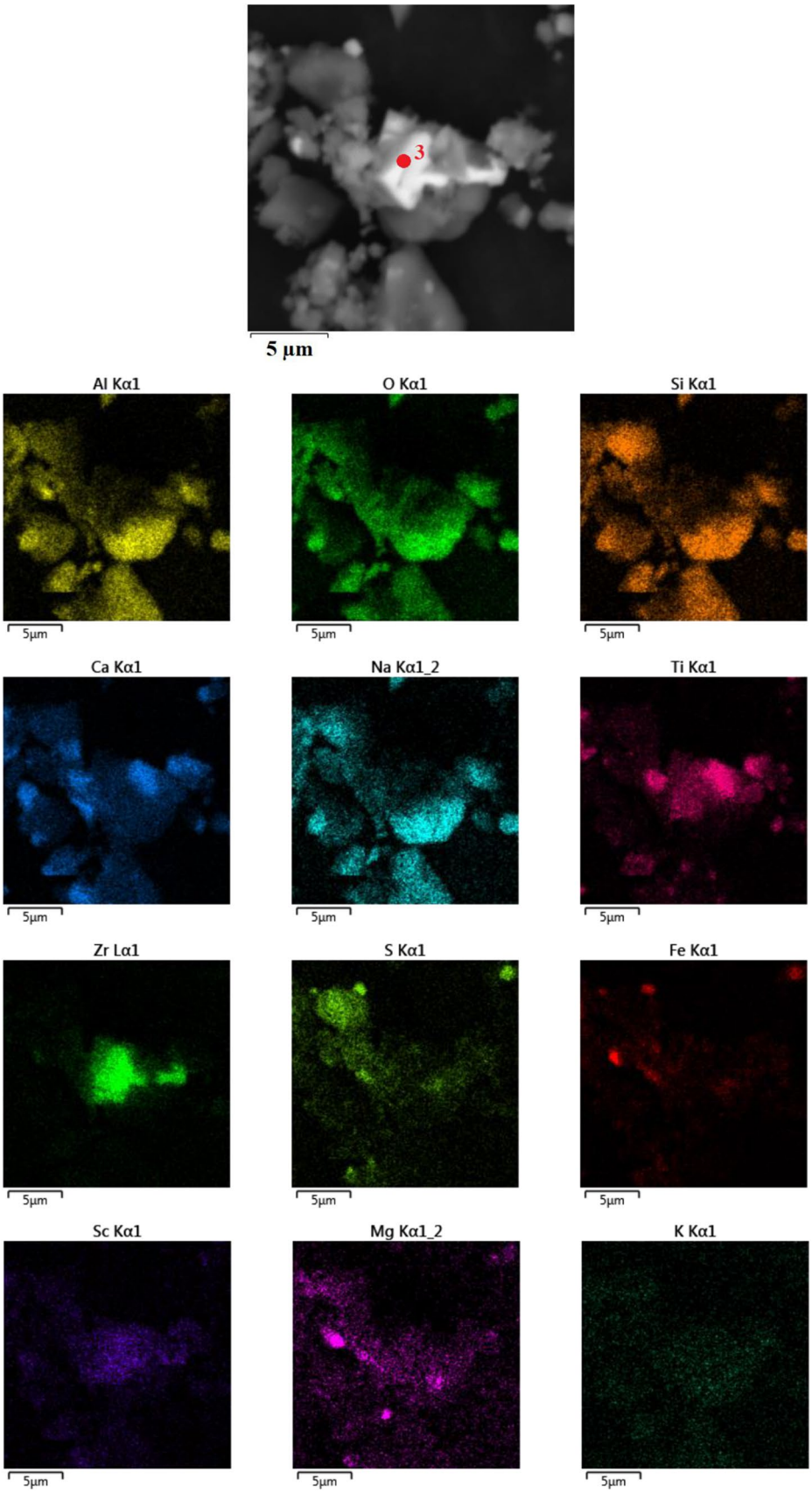

Fig. 12 SEM image with the distribution of elements in the tailings obtained after the roasting of the Bogoslovsky red mud with 18.2% Na_2SO_4 at 1150 °C for 1 h followed by wet magnetic separation

Conclusions

The experiments have confirmed that the addition of alkali metal salts can improve the iron extraction from red mud by the solid-phase carbothermic roasting at the temperature range of 1150–1350 °C followed by dry or wet magnetic separation. Moreover, the main parameters that affect the process are the additives amount, temperature, and red mud basicity (CaO/SiO_2). Basicity decreasing from 1.21 (Ural red mud) to 0.46 (Bogoslovky red mud) reduces the process temperature by 100–150 °C with obtaining a high iron recovery.

All the used additives, namely, Na_2SO_4, K_2SO_4, Na_2CO_3, and K_2CO_3, reduce the temperature of the appearance of the liquid phase during the roasting of red mud that has a positive effect on the iron recovery by subsequent magnetic separation. To be more precise, an increase of the liquid phase amount is beneficial for the iron recovery and iron concentrate grade, but the iron grade might tend to a slight decrease at the presence of high proportion of the liquid phase. Moreover, the addition of sodium salts leads to the appearance of liquid phase at lower temperatures than the addition of potassium salts does. Sulfates can both improve and hinder the iron extraction in the samples with a low and high basicity, respectively.

The concentrate obtained during the roasting with the addition of sulfates has a high sulfur content that is unfavorable for its use in steelmaking. From this point of view, application of carbonates is more beneficial than sulfates, although it has less impact on iron growth promotion. In addition, all the obtained concentrates have a high phosphorus content, which also deteriorates the quality of the concentrate in terms of use in steelmaking. The phosphorus content in the concentrate can be decreased by changing the roasting conditions, namely, the temperature and charge basicity, thereby hindering reduction of phosphorus-containing phases in red mud to remain them in the tailings after magnetic separation [63, 64]. The iron concentrate quality can also be improved by mechanochemical and nanochemical treatment, that is, ball milling of reduced red mud in the presence of sodium silicate and sodium hydroxide, which promotes separation of phosphorous compounds from the metallic iron surface [65].

The tailings from magnetic separation have an insignificant iron content and are suitable for extraction of scandium, aluminum, and titanium by hydrometallurgical methods. The tailings obtained by the roasting with the addition of potassium salts contain a certain part of aluminum in the form of water-soluble compounds that can be used for Al extraction without the application of corrossive solvents. The obtained tailings have a high content of alkali metals; it can be used not only for the extraction of valuable components, but also for obtaining of building materials. For example, bricks can be prepared by pressing of the mixture of tailings and slaked lime [66]. Moreover, the presence of alkali compounds in tailings can be promising to apply for obtaining alkali-activated inorganic materials such as geopolymers or inorganic polymers [67, 68].

Thus, carbothermic roasting with the addition of alkaline salts followed by dry or wet magnetic separation has proved to be a promising approach to extract iron from red mud. The application of the sodium salts is more beneficial for the iron extraction compared with the potassium salts, but potassium salts seem to be more promising in terms of subsequent Al extraction by leaching.

Acknowledgments The authors appreciate the Chemical Analytical Laboratory of the JSC "Design & Survey and Research & Development Institute of Industrial Technology" for chemical analysis.

Funding The present study was funded by RFBR according to the research project No. 18-29-24186. Access to the electronic database of scientific publications was provided within Russian state assignment No. 075-00328-21-00.

Declarations

Conflict of interest The authors declare that they have no conflict of interest.

References

1. Song Q, Li J, Zeng X (2015) Minimizing the increasing solid waste through zero waste strategy. J Clean Prod 104:199–210. https://doi.org/10.1016/j.jclepro.2014.08.027
2. Millati R, Cahyono RB, Ariyanto T et al (2019) Agricultural, industrial, municipal, and forest wastes. In: Taherzadeh M, Bolton K, Wong J, Pandey A (eds) Sustainable resource recovery and zero waste approaches, 1st edn. Elsevier B.V, St. Louis, Missouri, USA, pp 1–22
3. Binnemans K, Jones PT, Manjón Fernández Á, Masaguer Torres V (2020) Hydrometallurgical processes for the recovery of metals from steel industry by-products: a critical review. J Sustain Metall 6:505–540. https://doi.org/10.1007/s40831-020-00306-2
4. Rodriguez Rodriguez N, Machiels L, Onghena B et al (2020) Selective recovery of zinc from goethite residue in the zinc industry using deep-eutectic solvents. RSC Adv 10:7328–7335. https://doi.org/10.1039/d0ra00277a
5. Wang Z, Sohn I (2019) A review on reclamation and reutilization of ironmaking and steelmaking slags. J Sustain Metall 5:127–140. https://doi.org/10.1007/s40831-018-0201-5
6. Kumar S, Kumar R, Bandopadhyay A (2006) Innovative methodologies for the utilisation of wastes from metallurgical and allied industries. Resour Conserv Recycl 48:301–314. https://doi.org/10.1016/j.resconrec.2006.03.003
7. Lèbre É, Corder GD, Golev A (2017) Sustainable practices in the management of mining waste: a focus on the mineral resource. Miner Eng 107:34–42. https://doi.org/10.1016/j.mineng.2016.12.004
8. Zhang Z, Zhu Y, Yang T et al (2017) Conversion of local industrial wastes into greener cement through geopolymer technology:

a case study of high-magnesium nickel slag. J Clean Prod 141:463–471. https://doi.org/10.1016/j.jclepro.2016.09.147
9. Wiemes L, Pawlowsky U, Mymrin V (2017) Incorporation of industrial wastes as raw materials in brick's formulation. J Clean Prod 142:69–77. https://doi.org/10.1016/j.jclepro.2016.06.174
10. Seco A, Echeverría AM, Marcelino S et al (2020) Durability of polyester polymer concretes based on metallurgical wastes for the manufacture of construction and building products. Constr Build Mater 240: https://doi.org/10.1016/j.conbuildmat.2019.117907
11. Oliveira A, Martins CI, Castro F (2018) Incorporation of metallurgical wastes as inorganic fillers in resins. In: Vilarinho C, Castro F, Lopes ML (eds) WASTES: solutions, treatments, opportunities II, 4th edn. CRC Press, London, pp 403–408
12. Montoya-Bautista CV, Avella E, Ramírez-Zamora RM, Schouwenaars R (2019) Metallurgical wastes employed as catalysts and photocatalysts for water treatment: a review. Sustainability 118:2470. https://doi.org/10.3390/su11092470
13. Deus ACF, Bertani RM de A, Meirelles GC, et al (2019) The comprehensive utilization of steel slag in agricultural soils. In: Zhang YG (ed) Recovery and utilization of metallurgical solid waste. IntechOpen, pp 1–10. https://doi.org/10.5772/intechopen.81440
14. Matinde E, Simate GS, Ndlovu S (2018) Mining and metallurgical wastes: a review of recycling and re-use practices. J South African Inst Min Metall 118:825–844
15. Sidrak YL (2001) Dynamic simulation and control of the Bayer process. A review. Ind Eng Chem Res 40:1146–1156. https://doi.org/10.1021/ie000522n
16. Khairul MA, Zanganeh J, Moghtaderi B (2019) The composition, recycling and utilisation of Bayer red mud. Resour Conserv Recycl 141:483–498. https://doi.org/10.1016/j.resconrec.2018.11.006
17. Sutar H (2014) Progress of red mud utilization: an overview. Am Chem Sci J 4:255–279. https://doi.org/10.9734/acsj/2014/7258
18. Pascual J, Corpas FA, López-Beceiro J et al (2009) Thermal characterization of a Spanish red mud. J Therm Anal Calorim 96:407–412. https://doi.org/10.1007/s10973-008-9230-9
19. Reddy PS, Reddy NG, Serjun VZ et al (2021) Properties and assessment of applications of red mud (bauxite residue): current status and research needs. Waste Biomass Valoriz 12:1185–1217. https://doi.org/10.1007/s12649-020-01089-z
20. Joyce PJ, Björklund A (2019) Using life cycle thinking to assess the sustainability benefits of complex valorization pathways for bauxite residue. J Sustain Metall 5:69–84. https://doi.org/10.1007/s40831-019-00209-x
21. Joseph CG, Taufiq-Yap YH, Krishnan V, Li Puma G (2020) Application of modified red mud in environmentally-benign applications: a review paper. Environ Eng Res 25:795–806. https://doi.org/10.4491/eer.2019.374
22. Zeng H, Lyu F, Sun W et al (2020) Progress on the industrial applications of red mud with a focus on China. Minerals 10:773. https://doi.org/10.3390/min10090773
23. Das B, Mohanty K (2019) A review on advances in sustainable energy production through various catalytic processes by using catalysts derived from waste red mud. Renew Energy 143:1791–1811. https://doi.org/10.1016/j.renene.2019.05.114
24. Huangfu L, Abubakar A, Li C et al (2019) The utilization of red mud waste as industrial honeycomb catalyst for selective catalytic reduction of NO. R Soc Open Sci 6: https://doi.org/10.1098/rsos.191183
25. Orescanin V, Nad K, Valkovic V et al (2001) Red mud and waste base: raw materials for coagulant production. J Trace Microprobe Tech 19:419–428. https://doi.org/10.1081/TMA-100105056
26. Wang X, Zhang N, Zhang Y et al (2020) Multiple flocculant prepared with dealkalized red mud and fly ash: properties and characterization. J Water Process Eng 34: https://doi.org/10.1016/j.jwpe.2020.101173
27. Li X, Ji M, Nghiem LD et al (2020) A novel red mud adsorbent for phosphorus and diclofenac removal from wastewater. J Mol Liq 303: https://doi.org/10.1016/j.molliq.2019.112286
28. Deihimi N, Irannajad M, Rezai B (2018) Characterization studies of red mud modification processes as adsorbent for enhancing ferricyanide removal. J Environ Manage 206:266–275. https://doi.org/10.1016/j.jenvman.2017.10.037
29. Wang Y, Zhang T, Zhang Y et al (2019) Transformation and characterization of cement clinker prepared from new structured red mud by sintering. JOM 71:2505–2512. https://doi.org/10.1007/s11837-019-03475-y
30. Tang WC, Wang Z, Donne SW et al (2019) Influence of red mud on mechanical and durability performance of self-compacting concrete. J Hazard Mater 379: https://doi.org/10.1016/j.jhazmat.2019.120802
31. Kim Y, Lee Y, Kim M, Park H (2019) Preparation of high porosity bricks by utilizing red mud and mine tailing. J Clean Prod 207:490–497. https://doi.org/10.1016/j.jclepro.2018.10.044
32. Scribot C, Maherzi W, Benzerzour M et al (2018) A laboratory-scale experimental investigation on the reuse of a modified red mud in ceramic materials production. Constr Build Mater 163:21–31. https://doi.org/10.1016/j.conbuildmat.2017.12.092
33. Jitsangiam P, Nikraz H (2013) Sustainable use of coarse bauxite residue for alternative roadway construction materials. Aust J Civ Eng 11:1–12. https://doi.org/10.7158/14488353.2013.11463987
34. Akcil A, Akhmadiyeva N, Abdulvaliyev R et al (2018) Overview on extraction and separation of rare earth elements from red mud: focus on scandium. Miner Process Extr Metall Rev 39:145–151. https://doi.org/10.1080/08827508.2017.1288116
35. Binnemans K, Jones PT, Blanpain B et al (2015) Towards zero-waste valorisation of rare-earth-containing industrial process residues: a critical review. J Clean Prod 99:17–38. https://doi.org/10.1016/j.jclepro.2015.02.089
36. Xue SG, Wu YJ, Li YW et al (2019) Industrial wastes applications for alkalinity regulation in bauxite residue: a comprehensive review. J Cent South Univ 26:268–288. https://doi.org/10.1007/s11771-019-4000-3
37. Zhang TA, Wang Y, Lu G et al (2018) Comprehensive utilization of red mud: current research status and a possible way forward for non-hazardous treatment. In: Martin O (ed) Light metals 2018. The minerals, metals & materials series. Springer, Cham, Switzerland, pp 135–141
38. Dmitriev A (2019) The comprehensive utilisation of red mud utilisation in blast furnace. In: Recovery and utilization of metallurgical solid waste. IntechOpen, pp 1–10. https://doi.org/10.5772/intechopen.80087
39. RUSAL technology for extracting scandium. https://rusal.ru/en/innovation/technology/scandium-oxide/. Accessed 5 March 2021
40. Katyshev SF, Rukhlyadeva MS, Nikonenko EA et al (2015) Obtaining composite pigments from technogenic wastes from alumina production. Glas Ceram 72:303–305. https://doi.org/10.1007/s10717-015-9779-2
41. Borra CR, Blanpain B, Pontikes Y et al (2016) Smelting of bauxite residue (red mud) in view of iron and selective rare earths recovery. J Sustain Metall 2:28–37. https://doi.org/10.1007/s40831-015-0026-4
42. Valeev D, Zinoveev D, Kondratiev A et al (2020) Reductive smelting of neutralized red mud for iron recovery and produced pig iron for heat-resistant castings. Metals (Basel) 10:32. https://doi.org/10.3390/met10010032
43. Pepper RA, Couperthwaite SJ, Millar GJ (2016) Comprehensive examination of acid leaching behaviour of mineral phases from red mud: recovery of Fe, Al, Ti, and Si. Miner Eng 99:8–18. https://doi.org/10.1016/j.mineng.2016.09.012

44. Yang Y, Wang X, Wang M et al (2015) Recovery of iron from red mud by selective leach with oxalic acid. Hydrometallurgy 157:239–245. https://doi.org/10.1016/j.hydromet.2015.08.021
45. Gao F, Zhang J, Deng X et al (2019) Comprehensive recovery of iron and aluminum from ordinary bayer red mud by reductive sintering-magnetic separation–digesting process. JOM 71:2936–2943. https://doi.org/10.1007/s11837-018-3311-4
46. Eray S, Keskinkilic E, Varol M, et al (2020) A study on recovery of iron from red mud by solid state reduction followed by magnetic separation. In: Peng Z, Hwang JY, Downey JP, et al (eds) 11th International symposium on high-temperature metallurgical processing. Springer, Cham, Switzerland, pp 393–403. https://doi.org/10.1007/978-3-030-36540-0_35
47. Fofana M, Kmet S, Jakabsky S, et al (1995) Treatment of red mud from alumina production by high-intensity magnetic separation. Magn Electr Sep 6:243–251. https://doi.org/10.1155/1995/60564
48. Li Y, Wang J, Wang X et al (2011) Feasibility study of iron mineral separation from red mud by high gradient superconducting magnetic separation. Phys C Supercond Appl 471:91–96. https://doi.org/10.1016/j.physc.2010.12.003
49. Cardenia C, Balomenos E, Panias D (2019) Iron recovery from bauxite residue through reductive roasting and wet magnetic separation. J Sustain Metall 5:9–19. https://doi.org/10.1007/s40831-018-0181-5
50. Rao M, Zhuang J, Li G, et al (2016) Iron recovery from red mud by reduction roasting-magnetic separation. In: Sadler BA (ed) Light metals 2013. The minerals, metals & materials series. Springer, Cham, Switzerland, pp 125–130. https://doi.org/10.1007/978-3-319-65136-1_22
51. Chun TJ, Zhu DQ, Pan J, He Z (2014) Preparation of metallic iron powder from red mud by sodium salt roasting and magnetic separation. Can Metall Q 53:183–189. https://doi.org/10.1179/1879139513y.0000000114
52. Zhu DQ, Chun TJ, Pan J, He Z (2012) Recovery of iron from high-iron red mud by reduction roasting with adding sodium salt. J Iron Steel Res Int 19:1–5. https://doi.org/10.1016/S1006-706X(12)60131-9
53. Li G, Liu M, Rao M et al (2014) Stepwise extraction of valuable components from red mud based on reductive roasting with sodium salts. J Hazard Mater 280:774–780. https://doi.org/10.1016/j.jhazmat.2014.09.005
54. Grudinskii PI, Dyubanov VG, Zinoveev DV, Zheleznyi MV (2018) Solid-phase reduction and iron grain growth in red mud in the presence of alkali metal salts. Russ Metall 2018:1020–1026. https://doi.org/10.1134/S0036029518110071
55. Zinoveev D, Grudinsky P, Zakunov A et al (2019) Influence of Na_2CO_3 and K_2CO_3 addition on iron grain growth during carbothermic reduction of red mud. Metals (Basel) 9:1313. https://doi.org/10.3390/met9121313
56. Grudinsky P, Zinoveev D, Pankratov D et al (2020) Influence of sodium sulfate addition on iron grain growth during carbothermic roasting of red mud samples with different basicity. Metals (Basel) 10:1571. https://doi.org/10.3390/met10121571
57. Shiryaeva EV, Podgorodetskiy GS, Malyscheva TY, et al (2014) Influence of low alkaline red mud on the properties and microstructure of the agglomerates from the charge materials JSC "Ural steel." Izv Ferr Metall 57:14–19. https://doi.org/10.17073/0368-0797-2014-1-14-19
58. Bale CW, Bélisle E, Chartrand P et al (2016) Reprint of: FactSage thermochemical software and databases, 2010–2016. Calphad 55:1–19. https://doi.org/10.1016/j.calphad.2016.07.004
59. Tao J, Zheng L (2009) Determination of metallic iron in direct reduced iron by potassium dichromate titration after decomposition of sample by ferric chloride. Metall Anal 29:65–68
60. Parirenyatwa S, Escudero-Castejon L, Sanchez-Segado S et al (2016) Comparative study of alkali roasting and leaching of chromite ores and titaniferous minerals. Hydrometallurgy 165:213–226. https://doi.org/10.1016/j.hydromet.2015.08.002
61. Peckner D, Bernstein IM (1977) Handbook of stainless steels, 1st edn. McGraw-Hill, New York, USA
62. Vind J, Malfliet A, Bonomi C et al (2018) Modes of occurrences of scandium in Greek bauxite and bauxite residue. Miner Eng 123:35–48. https://doi.org/10.1016/j.mineng.2018.04.025
63. Yu W, Sun T, Kou J et al (2013) The function of $Ca(OH)_2$ and Na_2CO_3 as additive on the reduction of high-phosphorus oolitic hematite-coal mixed pellets. ISIJ Int 53:427–433. https://doi.org/10.2355/isijinternational.53.427
64. Bai S, Wen S, Liu D et al (2012) Beneficiation of high phosphorus limonite ore by sodium-carbonate-added carbothermic reduction. ISIJ Int 52:1757–1763. https://doi.org/10.2355/isijinternational.52.1757
65. Oleinik VO, Ablets EV, Panko AV, et al (2014) Influence of nanostructures on processes of solid-phase reduction and purification of ferrioxide—silicate materials. Met Noveishie Tekhnol 36:779–792. https://doi.org/10.15407/mfint.36.06.0779
66. Liu W, Yang J, Xiao B (2009) Application of Bayer red mud for iron recovery and building material production from alumosilicate residues. J Hazard Mater 161:474–478. https://doi.org/10.1016/j.jhazmat.2008.03.122
67. Hertel T, Pontikes Y (2020) Geopolymers, inorganic polymers, alkali-activated materials and hybrid binders from bauxite residue (red mud)—putting things in perspective. J Clean Prod 258: https://doi.org/10.1016/j.jclepro.2020.120610
68. Hertel T, Van den Bulck A, Blanpain B, Pontikes Y (2020) An integrated process for iron recovery and binder production from bauxite residue (red mud). Mater Lett 264: https://doi.org/10.1016/j.matlet.2019.127273

Authors and Affiliations

Pavel Grudinsky[1] · Dmitry Zinoveev[1,2] · Anfisa Yurtaeva[1,3] · Alex Kondratiev[2] · Valery Dyubanov[1] · Alexander Petelin[2]

[1] A. A. Baikov Institute of Metallurgy and Materials Science, Russian Academy of Science, Moscow, Russia 119334

[2] National University of Science & Technology "MISIS", Moscow, Russia 119049

[3] D. I. Mendeleev University of Chemical Technology of Russia, Moscow, Russia 125047